Description and comparison of 21st century thermosphere data

Bruinsma, Sean; Siemes, Christian; Emmert, John T.; Mlynczak, Martin G.

Important note
To cite this publication, please use the final published version (if applicable).
Please check the document version above.

Description and comparison of 21st century thermosphere data

Sean Bruinsma [a,*], Christian Siemes [b], John T. Emmert [c], Martin G. Mlynczak [d]

[a] *CNES, Space Geodesy Office, 18 Avenue E. Belin, 31401 Toulouse cedex 4, France*
[b] *Delft University of Technology, Faculty of Aerospace Engineering, Kluyverweg 1, 2629 HS Delft, the Netherlands*
[c] *Space Science Division, U.S. Naval Research Laboratory, Washington, DC 20375, USA*
[d] *Science Directorate, NASA Langley Research Center, Hampton, VA 23681, USA*

Abstract

The quality and distribution in time and space of available atmospheric observations are crucial for the accuracy of semi-empirical thermosphere models. However, datasets can be inconsistent, and their qualities and resolutions are often unequal. The main thermospheric density datasets of this century are briefly described and then compared to each other when possible in order to quantify differences. Total mass densities used in the comparisons include all high-resolution CHAMP, GRACE and GOCE data, Swarm A, daily-mean Stella, global daily mean TLE densities, and the SET HASDM density database. The temperature data from TIMED-SABER are also reviewed.

The recently updated daily-mean TLE densities (TLE2021) are 2–10 % smaller on average than the previous version (TLE2015). The differences are not constant offsets per altitude level, but fluctuations of up to 5 % are present. Compared to HASDM densities for 6 altitudes from 250 to 675 km, TLE2021 is 15–20 % smaller at 250 km, and then the difference diminishes with altitude to reach the same average value at 575 km. These mean differences also fluctuate by a few percent on time scales of months, to 10 % over half a solar cycle at 575 km. The TLE2021 and HASDM densities are larger than the accelerometer-inferred CHAMP, GRACE and GOCE densities and average offsets are 10–15 % and 10–20 %, respectively. The comparison to Swarm-A and Swarm-B showed mean offsets of 10 % and less, with significant positive trends seen in the comparison with HASDM. Finally, largest differences are found for Stella and HASDM at 800 km, up to 45 % with strong semiannual variations.

This study clearly shows that the available density data cannot be simply assimilated or combined without first accurately calibrating the data. The HASDM database is a valuable asset due to its considerable coverage in space and time, but its uncertainty and true resolution are not well understood and are still being evaluated. Data compatibility requires employing physically accurate and harmonized aerodynamic force models in the density derivation procedure, which is presently not achieved. The accuracy of the procedure, independent of the quality of the instrument (GNSS receiver, ground-based orbit determination, or accelerometer), inevitably decreases with altitude due to weakening of the drag signal to noise ratio.

The TIMED-SABER instrument provides measurements of pressure and temperature in the lower thermosphere. SABER temperature uncertainty is well-known. The SABER dataset now exceeds twenty years and has been continuously operating that entire time. It was ingested in NRLMSIS 2.0 and comparisons show the much-improved fit in comparison with NRLMSISE-00. The lower thermosphere temperatures significantly modify density at higher altitudes, and its measurement is essential for modeling and assessment.
© 2022 COSPAR. Published by Elsevier B.V. This is an open access article under the CC BY license (http://creativecommons.org/licenses/by/4.0/).

---

* Corresponding author.

E-mail addresses: sean.bruinsma@cnes.fr (S. Bruinsma), C.Siemes@tudelft.nl (C. Siemes), john.emmert@nrl.navy.mil (J.T. Emmert), m.g.mlynczak@nasa.gov (M.G. Mlynczak).

1. Introduction

Presently, thermospheric total mass density data sets can differ systematically by up to 30 %, even when they are derived from the same instrument at the same altitude. Similarly, different thermosphere models produce density predictions that differ by up to ∼30 %. The accuracy of semi-empirical thermosphere models depends largely on the quality and distribution in time and space of the available atmospheric observations, which are used to optimally fit the models' coefficients. Different databases were used in the construction of the COSPAR International Reference Atmosphere (CIRA) models NRLMSISE-00 (Picone et al., 2002), JB2008 (Bowman et al., 2008), DTM2013 (Bruinsma, 2015), NRLMSIS 2.0 (Emmert et al., 2020, shortened herein to 'MSIS 2.0') and DTM2020 (Bruinsma and Boniface, 2021). Unfortunately, the density data are not always consistent or of comparable quality and resolution. The objectives of this study are to characterize and compare the main upper atmospheric datasets since 2000 to each other (when possible), following a hiatus of more than 15 years in high-resolution data (e.g., since the Dynamics Explorer missions), in order to bring to light differences, inconsistencies and incompatibilities, and potential misunderstandings.

When developing a new thermosphere model, an important part of the effort resides in making the density datasets consistent and thereby compatible with the model, most often by means of estimating and then applying scaling factors to the data with respect to reference data. Inconsistencies are most often due to employing different approximations in the satellite models for shape, or for aerodynamic drag coefficients (Mehta et al., 2023). Data assimilation methods require a steady stream of observations with relatively high spatial and temporal resolution and known quality with which to update and refine model forecasts. As efforts are underway to advance thermosphere modeling with the development of data assimilation schemes that combine models and near-real-time observations (e.g., Codrescu et al., 2018; Sutton, 2018), it is judicious to analyze existing data and their differences in order to prepare for a future observing system and avoid unnecessary problems due to data inconsistencies. This International Space Weather Action Team (ISWAT; https://www.iswat-cospar.org) study constitutes one of the basic steps in the preparation of the update of the COSPAR Space Weather Roadmap, which this time will not omit the topic of thermosphere density and satellite aerodynamic drag. This study is especially timely and necessary due to the release of the new datasets SET HASDM database (Tobiska et al., 2021) and the globally averaged thermospheric density dataset of Emmert et al. (2021), and the imminent 20th anniversary of our main source of lower thermosphere data, TIMED (Russel III et al., 1999). The next section reviews the density data analyzed

in this study. The data comparisons are presented in Section 3. The summary and conclusions are given in Section 4.

2. Data

The CIRA models are all fitted to different density data, of which the main datasets that were acquired after 2000 will be described in this section. The backbone of the DTM2020 models is the complete CHAMP (Doornbos, 2011), GRACE (Bruinsma, 2015) and GOCE (Doornbos et al., 2014) high-resolution accelerometer-inferred density datasets, as well as Swarm-A densities (van den Ijssel et al., 2020). JB2008 was developed using 10 years of Air Force daily densities, 5 years output of the U.S. Space Force High Accuracy Satellite Drag Model (HASDM; Storz et al., 2005), 5 years of CHAMP and 4 years of GRACE data. NRLMSISE-00 was constructed with mass spectrometer, incoherent scatter radar, accelerometer, UV occultation, and various rocket measurements, along with global daily-mean orbit-derived thermospheric density and tabular lower atmospheric temperature. MSIS 2.0 additionally used extensive new lower and middle atmospheric temperature and composition observations, including TIMED/SABER temperatures, along with the TLE2015 daily-mean orbit-derived density described in Section 2.6. Mainly as a result of fitting to different data, or the same measurements but reprocessed, the CIRA models predict densities that are different within about 30 %.

Besides for modeling, the accelerometer-inferred densities in particular are essential to (semi-empirical and first principles) model assessment (Bruinsma et al., 2018, Bruinsma and Boniface, 2021). Fig. 1 presents the mean altitude of the satellites over their entire or ongoing missions (top frame), and the proxy for solar activity F10.7 (bottom frame). These datasets are described in the following subsections, which provide information on their processing schemes and models as well as spatial and temporal coverage and resolution.

2.1. CHAMP

The CHAMP (CHAllenging Mini satellite Payload; Reigber et al., 1996) satellite was in a near-polar and circular orbit from 2000 to 2010. The data covers the altitude range from initially 460 km to 260 km, though most data is collected above 320 km altitude as shown in Fig. 1. The 0.1 Hz accelerometer data, which results in a resolution along the orbit of about 80 km, were processed at TU Delft first by Eelco Doornbos (Doornbos, 2011), and later by Günther March (March et al., 2019). Both used slightly different high-fidelity satellite shape and aerodynamic coefficient models. The difference between the datasets is essentially a scale factor, the March et al. data being 5 ± 1 % larger than Doornbos', and the correlation varies
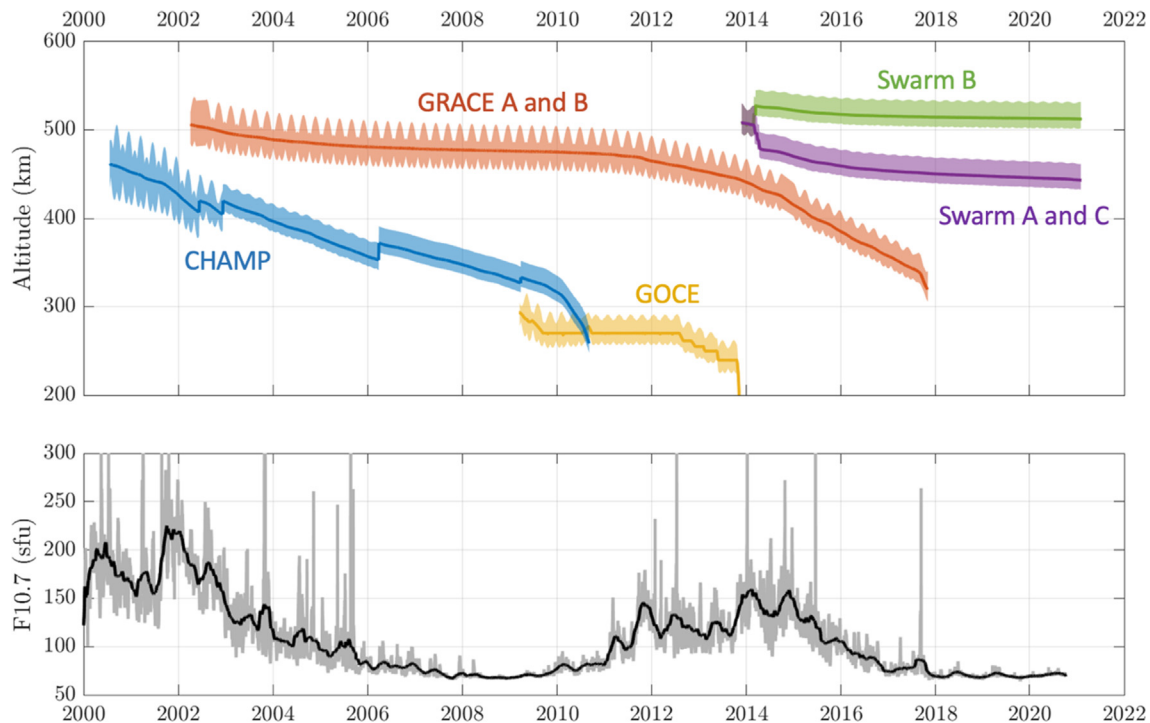
Fig. 1. Overview of altitude evolution of satellites carrying precise accelerometers (top) and F10.7 index as indicator of solar activity (bottom).

from 0.994 to 0.999. The Doornbos data is used in this study because it was used in previous studies for modeling as well as model assessment. The precision of the data was estimated at 1–4 % (Bruinsma et al., 2018).

2.2. GOCE

GOCE (Gravity field and steady-state Ocean Circulation Explorer; Drinkwater et al., 2003) was launched in March 2009 in a 96.5° inclination, dawn-dusk orbit, and re-entered the atmosphere in November 2013. Thanks to drag compensation, the orbit was maintained at 255 km mean altitude for the largest part of the mission, and then it was lowered in four stages ultimately to 224 km in May 2013. GOCE neutral density is an ESA product (https://earth.esa.int/eogateway/catalog/goce-thermosphere-data) with a resolution of about 80 km (10 s cadence) along the orbit and a precision of a few percent or better (Bruinsma et al., 2014). The processing of GOCE data (by TU Delft under ESA contract) was done using high-fidelity satellite shape and aerodynamic coefficient models, which led to the most accurate absolute density with an estimated precision of 1–3 % (Bruinsma et al., 2018). Version 1.5 is used in this study because it was used in previous works, in both thermosphere modeling (Bruinsma and Boniface, 2021) as well as model assessments (Bruinsma et al., 2018).

2.3. GRACE

Neutral densities inferred from accelerometer measurements of GRACE-A (Gravity Recovery and Climate Experiment; Tapley et al. 2004), which was in a near-polar and circular orbit, were computed for the entire mission using the methodology described in Bruinsma et al. (2004) and Bruinsma and Boniface (2021). The cadence of the measurements was 5 s, which leads to an along track resolution of about 40 km. Compared with the sophisticated TU Delft processing, the satellite shape was a simple model consisting of 8 flat plates, and the analytical Sentman aerodynamic coefficient model (Sentman, 1961) was employed. The GRACE data cover the period 08/2002 through 12/2016 (Fig. 1), but starting in 2011 2–3 gaps of 4 weeks each per year occurred and data quality was worse due to battery issues on the spacecraft. In order to make the GRACE data more consistent with the more accurate TU Delft densities, scaling factors were determined through comparison, after normalization to the mean altitude, with CHAMP and Swarm A densities when the orbital planes were nearly co-planar (less than 1-hour local time difference). The GRACE density scaling factors thus determined and applied in the adjustment of the thermosphere model DTM2020 (Bruinsma and Boniface, 2021) decrease over the mission: 0.76 (2002–2005), 0.73 (2006), 0.70 (2007–2016). The precision of this dataset is estimated at 2 % at high and 6 % at low solar activity (Bruinsma et al., 2018).

2.4. Swarm-A and Swarm-B

The ESA Swarm mission (Friis-Christensen et al., 2008), launched in November 2013, consists of three identical satellites (A and C side-by-side, and B in the higher orbit)

in near-polar and circular orbits at about 460 and 510 km after the initial deployment of the constellation in early 2014 (cf. Fig. 1). The GPS-derived densities (van den IJssel et al., 2020), again using high-fidelity satellite shape and aerodynamic coefficient models, are used in this study because of the serious problems and data gaps in the accelerometer data (Siemes et al., 2016). The densities are provided with 30 s cadence, but the spatial resolution and precision depend on the level of atmospheric drag experienced on orbit, and therefore principally on altitude and solar activity. The lowest precision was estimated at 5 % during low solar activity after averaging over one orbit (Bruinsma et al., 2018). The spatial resolution of the data was estimated to be approximately 4000–8000 km along the orbit when the F10.7 radio flux is larger than 100 sfu (solar flux units: 10^{-22} W m^{-2} Hz-^{1}).

2.5. Error sources in acceleration-derived density observations

Density observations can be derived from accelerometer measurements (Doornbos, 2011) as well as GNSS receiver data (van den IJssel et al., 2020). In a first step, we obtain the satellite's aerodynamic acceleration by reducing the effects of radiation pressure and thrust forces from the total nongravitational acceleration. Then, we derive the density observations from.

$$\boldsymbol{a} \cdot \boldsymbol{e} = \frac{1}{2}\rho v_r^2 \frac{A_{ref}}{m} \boldsymbol{C}_a \cdot \boldsymbol{e} \qquad (1)$$

where $\boldsymbol{a}$ is the aerodynamic acceleration (vector), ρ is mass density of the atmosphere, v_r is relative velocity (scalar) of the satellite with respect to the atmosphere, A_{ref} is the reference area, m is the mass of the satellite, $\boldsymbol{C}_a$ is the aerodynamic force coefficient (vector), and $\boldsymbol{e}$ is a suitably chosen unit vector. A suitable choice for vector $\boldsymbol{e}$ is the direction of the relative velocity vector, which requires that a three-dimensional acceleration is available. When this is not the case, e.g., because of an instrument malfunctioning as for CHAMP, we may choose vector $\boldsymbol{e}$ as the direction of the accelerometer axis that points approximately into the flight direction.

There are multiple errors that may affect acceleration-derived density observations, which we divide into four groups:

– Acceleration data calibration
– Modeling of the aerodynamic force coefficient
– Modeling of radiation pressure
– Wind models

A comprehensive assessment of the error sources is a challenging task and out of scope of this paper. Therefore, we provide in the following only an overview and indicate under which circumstances certain error sources are expected to play a role.

2.5.1. Acceleration data calibration

In case of electrostatic accelerometers, we need to calibrate their measurements, which typically encompasses the estimation of offsets and scale factors stemming from an imperfect voltage-to-acceleration conversion. Moreover, electrostatic accelerometers are sensitive to temperature changes. In case of the Swarm satellites (Siemes et al., 2016) and the GRACE satellites after deactivation of thermal control in April 2011 due to battery issues (Klinger and Mayer-Gürr, 2016), the offsets tend to follow the temperature variations. Uncertainties in the estimated scale factors are expected to be on the order of a few percent at most (van Helleputte et al., 2009; Visser and van den IJssel, 2016) and directly affect the scale of the density observations, independently of altitude and solar activity. In contrast, the uncertainty in the estimated offsets plays a role when the aerodynamic acceleration is small, which is the case at high altitudes and low solar activity.

2.5.2. Imperfect modeling of the aerodynamic force coefficient

The available modeling approaches for the aerodynamic force coefficient are well-explained by Mehta et al. (2014), Mostaza Prieto et al. (2014), and Livadiotti et al. (2020). The aerodynamic force coefficient is first and foremost a function of the satellite's geometry and orientation with respect to the flight direction. March et al. (2019) demonstrated that using high-fidelity geometry models instead of panel models reduces errors by about 10 % of the density. Further, the aerodynamic force coefficient depends on the atmospheric temperature and composition (Doornbos, 2011). Since all accelerometer-carrying satellites launched since 2000 are not equipped with sensors for measuring atmospheric temperature and composition, we rely on thermosphere models. For lack of information, we assume commonly that gas-surface interactions are independent of the properties of satellite surface materials, though new surface coatings currently under development might invalidate this assumption in the future (Crisp et al., 2021). From Eq. (1) it is obvious that the errors in the aerodynamic force coefficient result in an incorrect scaling of the densities. The scale error is on the order of 10 % and not constant, varying with the atmospheric temperature and composition used, and is mainly a function of the gas-surface interaction model selected. Mehta et al. (2023), in this same special issue, will elaborate this aspect in detail. It notably leads to differences not only between data sets from different satellites, but also between density data sets inferred from the same data of ±10 %. In this study, only one data set per satellite is analyzed since the main effect for such cases is in the form of an offset.

2.5.3. Inaccurate modeling of radiation pressure

As for the modeling of the aerodynamic coefficient, errors resulting from usage of panel models instead of high-fidelity geometry models are on the order of 10 % (Wöske et al. 2019). Moreover, many authors neglected

in the past the effect of the satellite's thermal radiation, which notably contributes to the total radiation pressure (Vielberg and Kusche, 2020). A significant source of uncertainty in radiation pressure modeling is the thermo-optical properties of the satellite surfaces, including their changes over time due to aging effects. Overall, we may expect errors in radiation pressure modeling of 10–30 %. Radiation pressure is a force that is practically independent of altitude and solar activity. Thus, such errors play a role when the aerodynamic acceleration is small, i.e., at high altitudes and low solar activity. For instance, van den IJssel et al. (2020) argue that radiation pressure model errors are a significant error source for Swarm density observations during the solar minimum between cycle 24 and 25, in particular for the higher-flying Swarm B satellite. The radiation pressure in this study was modeled according to Doornbos (2011), using the information provided for CHAMP by Lühr et al. (2002), for GRACE by Bettadpur (2012), for GOCE by Doornbos et al. (2014), and for Swarm by Siemes (2019). Fig. 2 displays the ratios of orbit-averaged solar radiation pressure over the aerodynamic accelerations of GOCE, CHAMP, GRACE-A (the full range from solar maximum to solar minimum, i.e. from 2002 to 2009), Swarm-A and Swarm-B. The ratios reach 100 % and larger, i.e. radiation pressure is equal to or larger than atmospheric drag. We expect that density observations from GRACE in the solar minimum between cycles 23 and 24, and Swarm in the solar minimum between cycles 24 and 25, are notably affected by errors in radiation pressure modeling.

2.5.4. Wind model errors

The relative velocity v_r includes winds, the velocity of the atmosphere corotating with Earth, and winds. Though winds are much smaller than the satellite velocity of about 7.6 km/s, head and tail winds can still significantly change the relative velocity. For instance, 40–400 m head or tail winds cause a 1–10 % change in relative velocity. From Eq. (2) follows that a change in relative velocity has the same effect on the aerodynamic acceleration as a change in density. Since the satellites carrying accelerometers are not equipped with wind sensors, we use models such as

the Horizontal Wind Model (HWM, Drob et al., 2015) to account for winds. Since there are hardly any in-situ wind measurements in the altitude range of 300–500 km, we should expect imperfections of the wind models in that altitude region. During geomagnetic storms, we may expect peak winds up to 800 m/s (Sutton et al., 2005), which are difficult to predict by models and, consequently, may cause errors in the density observations up to 20 % locally.

2.6. TLE daily-mean global densities

Two versions of orbit-derived, global-average daily-mean densities are evaluated in this study: the datasets described by Emmert (2015) (herein denoted 'TLE2015') and Emmert et al. (2021) ('TLE2021'). The TLE2015 dataset is derived from the operational archive of two-line orbital element sets (TLEs); it applies the techniques of Picone et al. (2005) and Emmert (2009) to ~5000 objects. The dataset covers the years 1967–2013 and altitudes 250–575 km. The estimated precision of the global averages is typically 1 %–2 % for the time period covered by this study (i.e., after 2000). The data are provided at daily cadence, but the temporal resolution is 3–4 days, due in part to the fact that the fit span of the underlying TLEs is typically ~3 days, and in part because the data are smoothed to that resolution as part of the density retrieval procedure.

The newer orbit-derived dataset, TLE2021, uses a new approach (Emmert et al., 2021) for estimating the orbital energy loss due to orbital drag. For years 2001 and after, archived operational Special Perturbations (SP) state vectors are used for this purpose, instead of TLEs (in this approach, TLEs are still used to estimate the orbital path needed to calculate the work done by non-conservative forces). As a result, the typical precision is improved to ~0.5 %–1.5 %. The new dataset was otherwise produced using the same techniques for combining many objects (~7700 for TLE 2021) as TLE2015; it covers the years 1967–2019, with the same altitude coverage and temporal resolution as TLE2015. The two datasets are offset by ~8 % on average (TLE2021 has lower densities), due to a revised estimate in TLE2021 (following Pilinski et al., 2011) of the ballistic coefficient of the primary reference
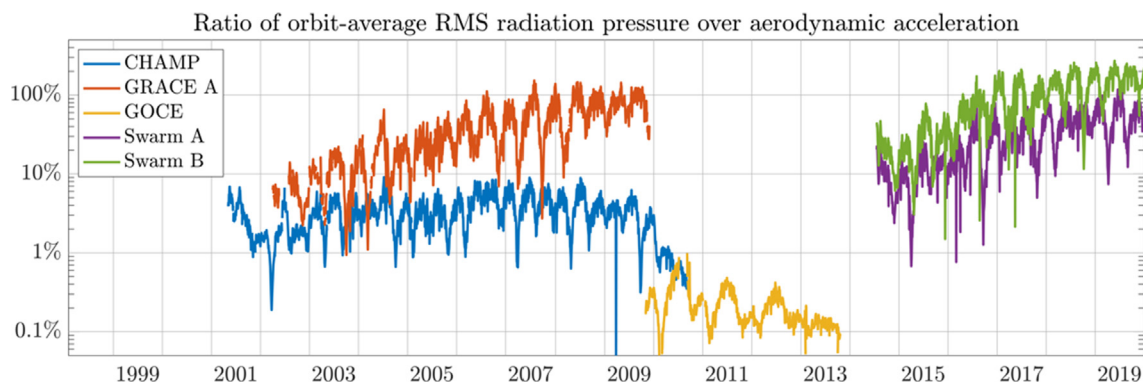

Fig. 2. Ratios of radiation pressure over aerodynamic accelerations for GOCE, CHAMP, GRACE-A, Swarm-A and Swarm-B.

object (Starshine I). The accuracy of TLE2021 was estimated to be 5 %–10 %, due to remaining uncertainties in theoretical ballistic coefficients and limitations of the method.

2.7. Stella

The spherical satellite Stella is in a 96° inclination and circular orbit at approximately 813 km altitude. Because of its shape (no attitude-related errors), knowledge of the satellite characteristics (mass, surface, reflectivity), and the very accurate laser tracking by the International Laser Ranging Service (ILRS; Pearlman et al., 2002), it is suitable for density derivation despite its relatively high altitude. Daily-mean densities were inferred from the analysis of orbit perturbations (following Jacchia and Slowey, 1963), which essentially ties the observed decay to a mean density over the orbit, spanning the period 2000–2019. It is difficult to estimate precision and accuracy of these daily-mean densities, but the former is estimated at 5–20 % (high - low solar activity) based on orbit adjustment tests (Bruinsma et al., 2018).

2.8. SET HASDM density database

Space Environment Technologies (SET) has made available 20 years of densities through the SET HASDM Database (Tobiska et al., 2021), which is derived from the U.S. Space Force High Accuracy Satellite Drag Model (Storz et al., 2005). The HASDM data assimilation system modifies the JB2008 model densities using a dynamic calibration of the atmosphere (DCA) with a segmented solution approach. This approach extracts the time resolution needed to accurately determine the dynamically changing thermospheric density by taking a 3-h sub-interval within the fit span of an estimated 1.5-day interval for each of up to 90 calibration satellites. Densities are given every 3 h from 2000 to 2019 on equiangular grids extending from pole to pole [10° latitude × 1hr local time], and from 175 to 825 km altitude in steps of 25 km. A variable aerodynamic coefficient was used in the processing of the numerous objects.

The 1-σ precision is shown per year on the SET website (https://spacewx.com/hasdm/) and in proceedings (https://amostech.com/TechnicalPapers/2021/Poster/Tobiska.pdf) and ranges from 2 to 11 %, which is based on the analysis of calibration satellites and comparison with the HASDM density dataset. The displayed precisions as a function of altitude present unexplained and unexpected minimums, notably around 600–650 km despite the high relative contribution of solar radiation (Section 2.5), and maximums. A comparison with CHAMP and GRACE densities was done by Licata et al. (2021). While work has been done to describe the characteristics and uncertainty of the data, this remains an open area of active research in the community. Only the HASDM database can be directly compared

with all other density datasets, and as such it is valued asset.

2.9. TIMED-SABER

SABER measures approximately 1400 profiles of infrared limb radiance in 10 different spectral channels from 400 km to the Earth's surface each day. From these radiance profiles the many SABER data products (temperature, ozone, water, carbon dioxide, atomic species, energetics) are derived. The approximate spatial resolution between profiles is about 3.2°in latitude. The TIMED satellite which hosts SABER is in an orbit inclined 74°to the equator. SABER views normal to the velocity vector and observes a range of latitude from 83° in one hemisphere to 53° in the other. The hemispheric latitude range alternates every 60 days as the TIMED spacecraft rotates 180 degrees in azimuth to keep SABER on the 'cold' (antisunward) side. SABER samples all local times over a period of 60 days. The instrument has been recording data continuously since it began science operations in late January 2001.

Most important for the thermosphere models are the vertical profiles of neutral kinetic temperature from 15 km to 110 km, which are determined from measurements of infrared limb emission from vibration-rotation transitions of the CO_2 molecule in the spectral interval 13.1 μm to 17.2 μm.

(760 cm^{-1} to 580 cm^{-1}) described by Mertens et al. (2001). SABER also requires the vertical profile of CO_2 concentration (or mixing ratio) to retrieve temperature (Rezac et al., 2015. SABER produces two versions of neutral kinetic temperature. An 'operational' version (currently numbered Version 2.07) in which the CO_2 concentration is provided from the WACCM model (Whole Atmosphere Community Climate Model; Marsh et al., 2013) and for which temperature profiles are retrieved both day and night. Uncertainties in the SABER operational temperatures are discussed in Remsberg et al. (2003, 2008) and Garcia-Comas et al. (2008). Specifically, Garcia-Comas et al. note that the Version 2.07 SABER temperatures at 104 km, approximately the height of the 10^{-4} hPa pressure surface are uncertain by as much as 8.3 K. However, the temperature (and hence density) uncertainty is much smaller below that altitude but are also much larger above, increasing to approximately 29 K at 110 km. Observed SABER global mean temperatures at 104 km range from 200 K to 225 K. The uncertainty in temperature then corresponds to an uncertainty in density of 3.6 % to 4.2 % for this range of temperatures. An additional version (Rezac et al., 2015) provides temperatures and CO_2 concentrations in the daytime and uses CO_2 concentrations simultaneously derived from a combination of SABER's CO_2 emission channel at 4.3 μm and the 15 μm channels. The two techniques are comparable although as noted by Rezac et al. (2015) "The two-channel retrieved temperatures exhibit very similar spatial variability com-

pared to the SABER operationally retrieved but are generally colder in the broader region around mesopause, especially in the polar summer hemisphere by 5–12 K, as a result of higher CO_2 retrieved. An exception to the generally colder temperature profiles is the high latitudes during the equinox seasons." Uncertainties on the Rezac et al. (2015) temperature and density profiles should be comparable to those of the operational SABER retrievals. The Rezac et al. temperature profiles extend to a pressure surface of 5×10^{-4} hPa, approximately 95 km altitude.

3. Comparisons

The comparisons are done on the following quantities:

- Daily-mean densities
- Densities along the orbit

Density data are evaluated by computing the mean, and standard deviation (StD) when pertinent, of the density ratios in natural log space (ln(O/C)) and then converting back to ratio space. The metrics are described in (Bruinsma et al., 2018). When density data are not at exactly the same altitude z, one or both datasets must first be normalized to a reference altitude z_0. This is accomplished using a thermosphere model density ρ_M according to Eq. (2) below:

$$\rho(z_0) = \rho(z) \frac{\rho_M(z_0)}{\rho_M(z)} \qquad (2)$$

The normalization process is not error free, especially if altitude differences exceed 50 km, and the result depends on the model employed to a varying and sometimes large extent (differences may exceed 5 %). For that reason, it was only used in the comparison of Stella and HASDM densities at 800 km, because only for that satellite the impact of the normalization was very small, as will be shown in Section 3.4.

The SABER temperatures cannot be compared in a similar way due to the scarcity of other data in the lower thermosphere, which is why their uncertainty was discussed in some more detail in Section 2.9. The lower thermosphere temperatures have a significant impact on densities at higher altitudes, and we present comparisons with MSIS in Section 3.5.

3.1. TLE2015, TLE2021 and HASDM at 250, 325, 375, 400, 475, and 575 km

The TLE2021 data are compared with TLE2015 and HASDM densities for six altitudes. The comparison starts on 1 January 2000 and covers 13 and 20 years of data, respectively. The global daily-mean of the HASDM densities is computed on each of the six altitude levels using all data per day, and applying latitude weighting (using sqrt(cos(latitude)) as weights). As an example, Fig. 3 shows the densities from 2000 to 2019 at 250 km, which clearly shows that offsets between the datasets are present.

The offsets are better made visible by calculating ratios per day and then smoothing over 81 days. This is displayed in Fig. 4 for TLE2021/TLE2015 (top frame) and HASDM/TLE2021 (bottom frame). The offsets are not constant, but variable on time scales of months to years. At 250 km, the TLE2021 densities are up to 11 % smaller than TLE2015. At 575 km, the mean offset is smallest, but the variability is highest, and a large dip of about 4 % is revealed for 2013. Excepting the 250-km level, there are shifts in the offsets, e.g. at 475 km from 0.945 in 2000 climbing to about 0.97 in 2011, as well as a transient enhancement to ~ 0.99 in 2012. As discussed in Emmert et al. (2021, Section 4), these shifts are possibly due to the fact that in the TLE2015 dataset, no new objects were introduced after 2007.

The density ratios displayed in Fig. 4, bottom frame, reveal offsets evolving from largest at 250 to smallest at 575 km, similar but larger to those in Fig. 4, top frame (TLE2021 densities are up to 22 % smaller than HASDM). The StD is highest again at 575 km, but the smallest variations are seen now at 375 km. The density ratios above and below 375 km present a slow variation following the solar cycle, and most notably the deep solar minimum from 2007 to 2010, but with opposite progression.

The smaller HASDM/TLE2021 ratios at higher altitudes mean that HASDM density falls off more steeply with increasing altitude than TLE2021, which implies that the effective HASDM temperature is lower than that of TLE2021, an effect that is amplified at solar minimum. This difference is possibly caused by the way the orbit data is assimilated in the two methods. HASDM adjusts the JB2008 thermosphere temperature parameters and assumes the JB2008 density and composition at 125 km is correct, whereas TLE2021 fits observed/NRLMSISE-00 density ratios as a function of height, with no constraints on density at 125 km. The TLE2021 approach thus accommodates density and composition variations and offsets at $\sim$120 km (e.g., due to temperature variations at lower altitudes) that project directly to higher altitudes. Different methods of ballistic coefficient determination may also contribute to the temporal dependence of the HASDM/TLE2021 ratios: TLE2021 ballistic coefficients are calibrated to a theoretical value for a single reference object, whereas HASDM ballistic coefficients are a long-term average of the fitted ballistic coefficients for each object, which assumes that the reference model (JB2008) is unbiased.

The strongest solar cycle signature of more than 10 % is seen at 575 km, which also presents outlying peaks between 2008 and 2010, and in 2019. The first and highest peak in 2008 is similar to, but much larger than, a dip seen in Fig. 4, bottom frame. Comparison to HASDM at 575 km for 2013 does not show unusual variation, which means that the TLE2021 densities for that year are not the cause of the large dip seen in the TLE2021/TLE2015 density ratios. The peak in 2019 cannot be traced here
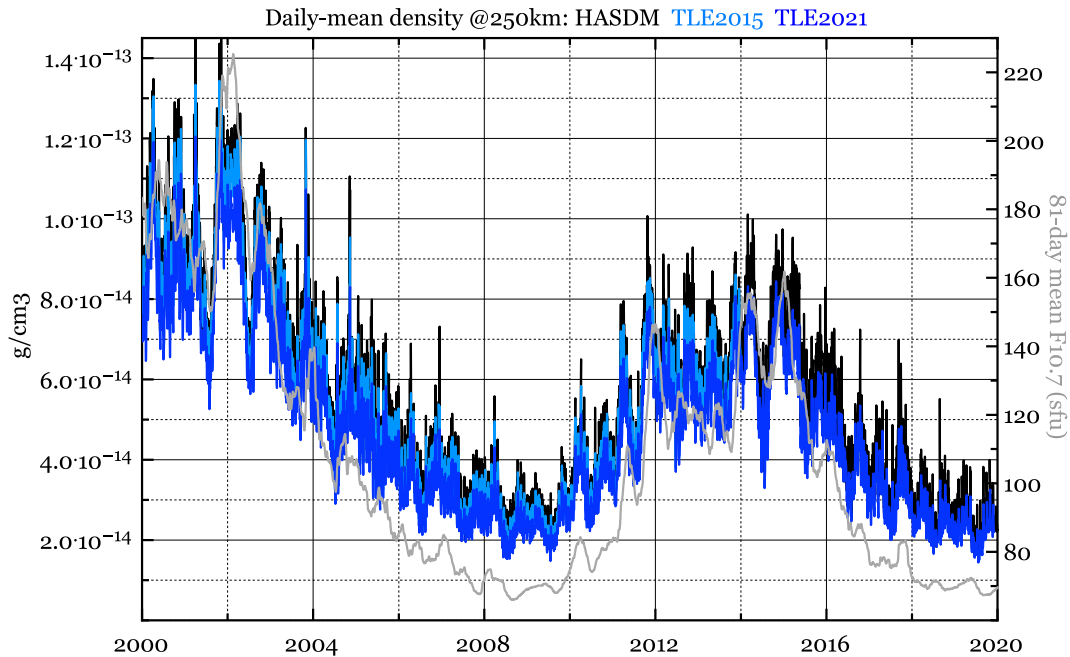
Fig. 3. The daily-mean TLE2015, TLE2021 and HASDM densities at 250 km, and the 81-day mean F10.7 index (grey; right axis).

due to absence of a third dataset. The solar cycle signature at 250 km is weaker than at 575 km, but still reaches about 5 % from 2000 to 2008.

3.2. TLE2021 and CHAMP, GRACE, GOCE and Swarm

The global daily-mean TLE2021 densities, after interpolating to the appropriate orbital altitudes, are compared with CHAMP, GRACE, GOCE and Swarm data. Fig. 5 displays the observation-to-TLE2021 density ratios (top frame) and standard deviations (middle) smoothed over 81 days, and the daily and 81-day smoothed F10.7 solar activity index (bottom frame). As TLE densities are averaged over all local times (i.e., a global mean) whereas the satellites sample basically the two local times of their precessing orbit planes, the undulations in the ratios correspond to the periods needed to cover all local times, e.g. 4.4 months for CHAMP and Swarm-A. GOCE density ratios present only an annual variation because the local time plane of its orbit only changed by two hours over the entire mission. The TLE2021 densities are on average 5–15 % larger than the satellite observations. GRACE densities agree least with TLE2021, and the density ratios not only present strong trends (e.g., from 2008 to 2011) but also two relatively constant levels from 2003 to 2008 and then from 2011 to 2016. In 2002 and 2017 the ratios are significantly different, most likely due to inaccurate accelerometer calibration. The offsets are smallest for Swarm-B and Swarm-A (5–6 %, respectively).

Standard deviations grow much faster for Swarm-B than Swarm-A because of the lower drag at the higher Swarm-B altitude, resulting in much larger errors in the

densities due to inaccuracies in solar radiation pressure modeling.

3.3. HASDM and CHAMP, GRACE, GOCE and Swarm densities along orbits

The GOCE, CHAMP, GRACE-A, Swarm-A and Swarm-B densities can be compared along their orbits to HASDM after interpolating to the orbit positions (altitude, latitude and local time). Fig. 6 displays the observed-to-HASDM density ratios (top frame) and standard deviations (middle) using orbit-averages smoothed over 81 days, and the daily and 81-day smoothed F10.7 solar activity index (bottom frame). HASDM densities are on average 3–21 % larger than the satellite densities. Except for the GOCE density ratios, trends are visible too. CHAMP shows a decreasing trend of 0.85 to 0.80 over 9 years, whereas Swarm-A and Swarm-B climb approximately 0.05. The trends appear to be correlated with the decaying phases of the solar cycles 23 and 24. As for TLE2021 data, the GRACE densities agree least with HASDM, and similar trends and levels as seen Fig. 5 are revealed. In 2002 and 2017 the ratios are significantly different too. It is therefore most likely that the GRACE data are affected by several types of errors. Waves in the ratios as seen in Fig. 5 when comparing with the TLE2021 densities are not or hardly present, which means that the large-scale local time variations are accurately captured.

The standard deviations are clearly inversely proportional to solar activity, for reasons explained in Section 2.5 and shown in Fig. 2. As in Fig. 5, Swarm-B and Swarm-A standard deviations present the same increasing trend
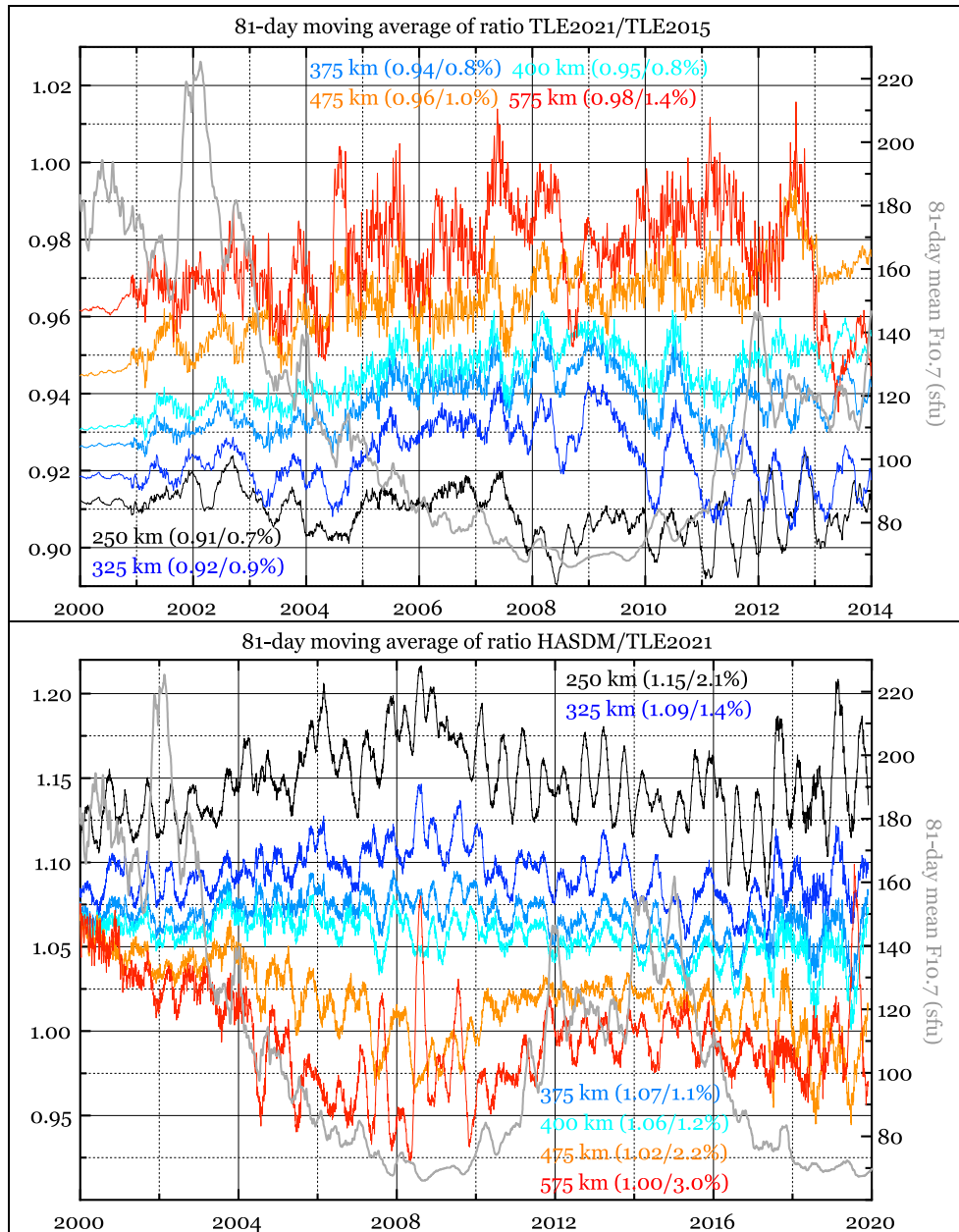
Fig. 4. The smoothed ratios TLE2021/TLE2015 and HASDM/TLE2021 (bottom frame), and the 81-day mean F10.7 index (grey; right axis). The mean and StD of the ratios are given for each altitude.

towards solar cycle minimum due to larger errors in the densities caused by inaccuracies in solar radiation pressure modeling. The higher standard deviation for the GOCE density ratios at the very beginning of the mission is due to higher noise in the thruster data at very low thrust levels. Compared to Fig. 5, standard deviations are much smaller. This also is due to comparing densities for identical local times, which consequently are in good agreement.

3.4. Stella and HASDM 800 km

The Stella densities were normalized to 800 km using NRLMSISE-00, JB2008 and DTM2020. Then, the ratios

HASDM/Stella at 800 km were computed using daily mean densities, which are smoothed over 81 days. This is shown in Fig. 7. The differences due to normalization with three different models are negligible for Stella. HASDM densities are up to 40 % larger than Stella densities, but also smaller in the interval 2012–2016. The ratios vary much more than those calculated at lower altitudes, and this is most likely due to a combination of errors in solar radiation pressure modelling and aerodynamic coefficient modeling. Negative correlation with solar activity is seen from 2004 to 2020, but not for the maximum of solar cycle 23 from 2000 to 2003. The large differences between Stella and HASDM densities at 800 km are not understood presently.
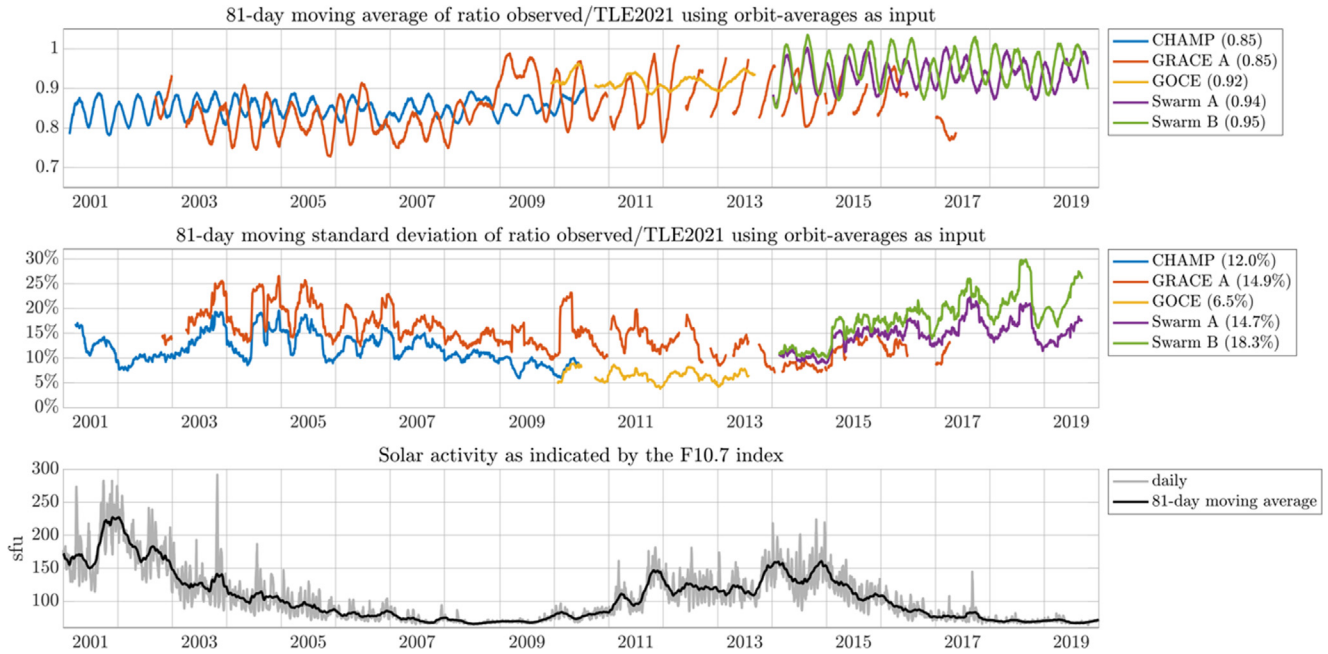
Fig. 5. Orbit-averaged observed/TLE2021 density ratios smoothed over 81 days for CHAMP, GRACE, GOCE, Swarm-A, and Swarm-B. Mean density ratios and StD are given in parentheses.
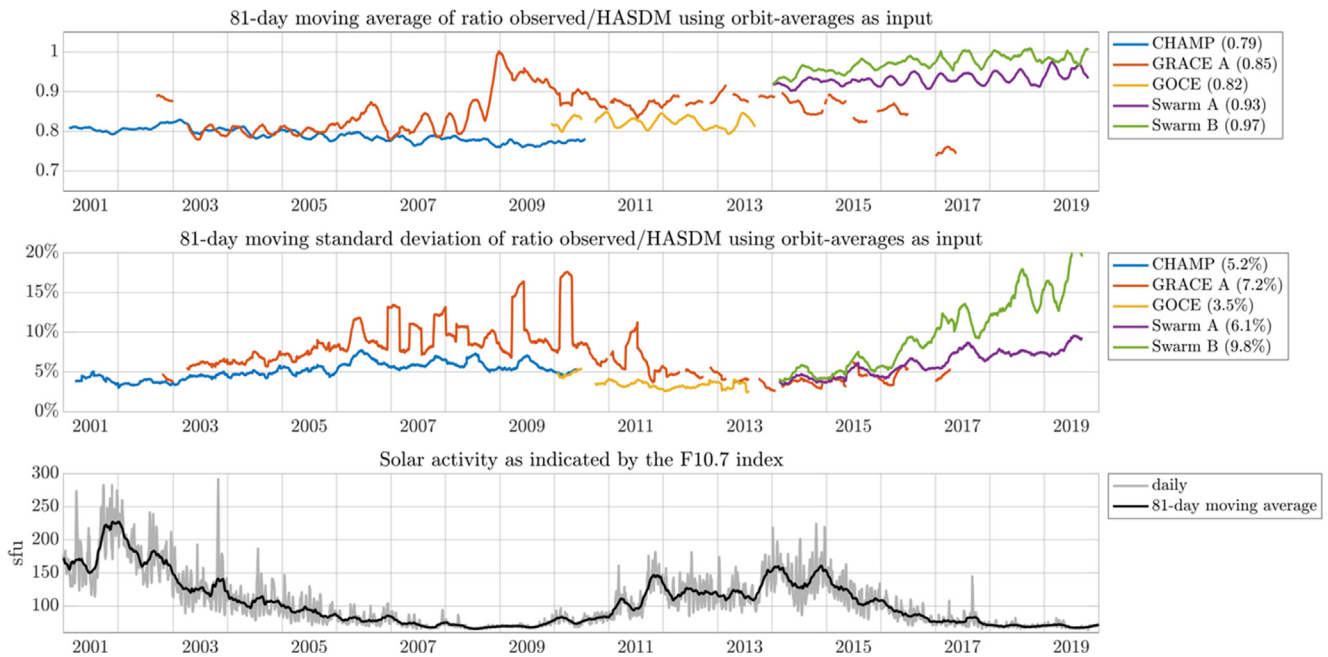

Fig. 6. Orbit-averaged observed/HASDM density ratios smoothed over 81 days for CHAMP, GRACE, GOCE, Swarm-A, Swarm-B. Mean density ratios and StD are given in parentheses.

3.5. SABER and MSIS at 100 km

Dawkins et al. (2018) have conducted the most in-depth evaluation of the SABER temperatures in the upper mesosphere and lower thermosphere (75 km to 105 km) in comparisons with lidar observations on a seasonal basis at nine different locations representing widely different latitudes. The differences between SABER and the lidar data typi-cally were found to be within the respective uncertainties of the measurements over the range of altitudes examined. However, at and above 100 km, SABER did indicate a warmer temperature than the lidar observations. In addi-tion, SABER data were typically warmer in the polar sum-mer mesosphere than the lidar observations. The comparisons are summarized in Table 3 of Dawkins et al. Continuous comparisons over longer periods (years to
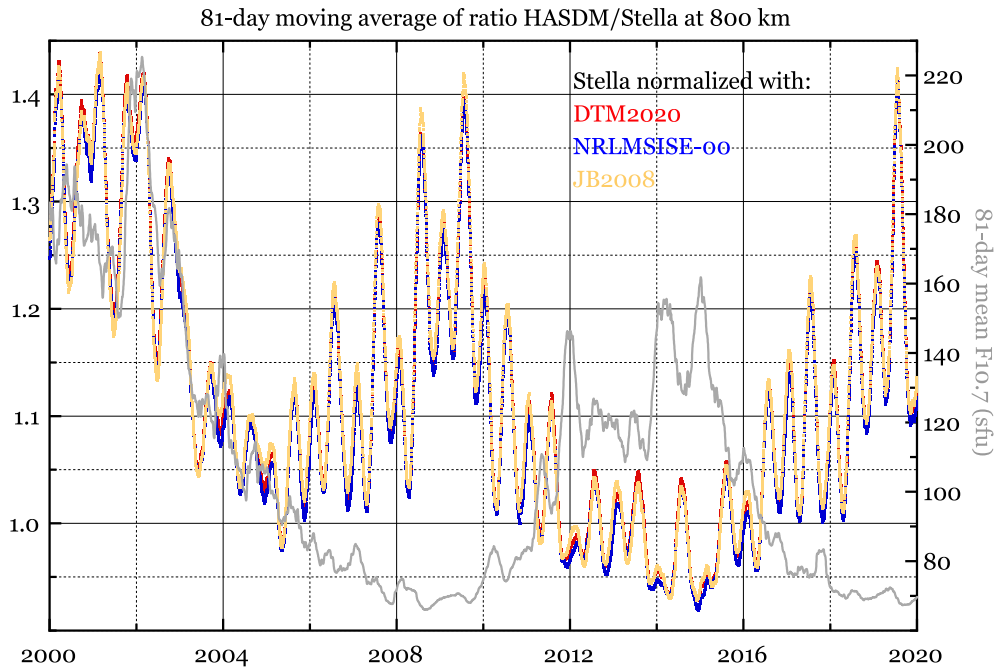
Fig. 7. 81-day moving average of HASDM/Stella density ratios at 800 km, and the 81-day mean F10.7 index (grey; right axis). The Stella densities were normalized with 3 models, with negligible difference.

decades) of SABER and correlative measurements are not available. We therefore compare SABER observations with the new MSIS 2.0 model temperatures. The DTM and JB2008 models cannot be used in this comparison because both start at 120 km altitude. Fig. 8 shows averaged and smoothed SABER v. 2.07 temperatures (red) and corresponding point-for-point averages of MSIS 2.0 (blue) and MSISE-00 (green) temperatures at the SABER measurement times and locations.

Temperature perturbations around 100 km altitude have a sizeable effect at higher altitudes. A temperature perturbation of 1 K near 100 km altitude that persists over a 10 km height range will produce a $\sim 1\%$ perturbation in density at higher altitudes, due to hydrostatic adjustment,

as follows. Locally, density decreases exponentially with altitude according to a scale height H that is proportional to temperature:

$$\rho = \rho_0 \exp\left(-\frac{z-z_0}{H}\right)$$
$$H = \frac{RT}{Mg}$$

where $R \cong 8.314$ J/K/mol is the universal gas constant, T is temperature, $\bar{M}$ is the mean molar mass, and g is gravitational acceleration. Given a temperature perturbation of δT, and assuming the other parameters are constant over the height interval (z_0, z),
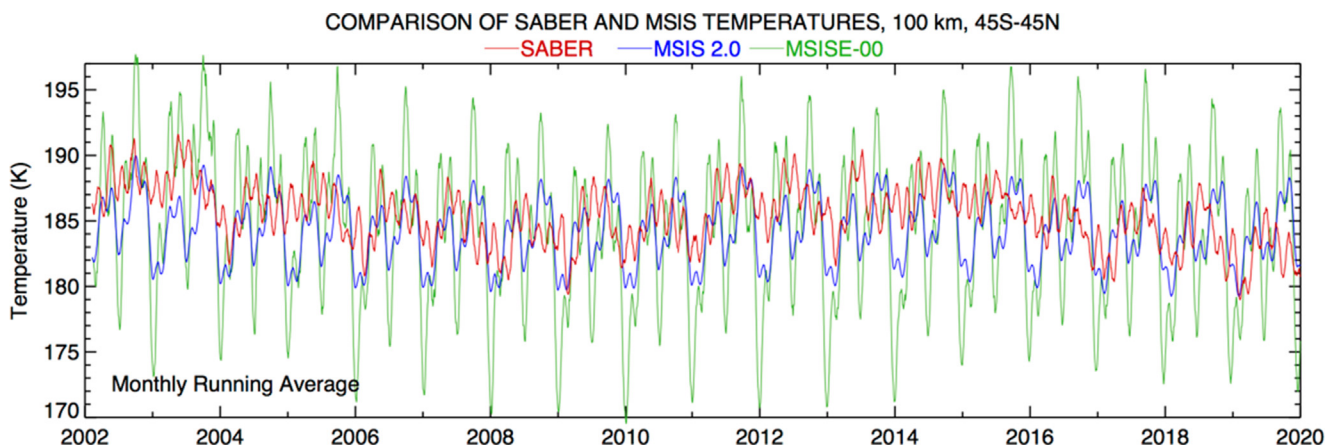

Fig. 8. (red) SABER v. 2.07 temperatures, first averaged over altitudes from 97.5 km to 102.5 km and latitudes from 45S to 45 N and then smoothed with a monthly running average. A random sample of 2.5 % of the SABER database was used for the analysis. (blue) Corresponding point-for-point averages of MSIS 2.0 temperatures at the SABER measurement times and locations. (green) Corresponding point-for-point averages of NRLMSISE-00 temperatures.

$$\delta(\ln \rho) = \frac{z - z_0}{H^2} \delta H = \frac{z - z_0}{H} \frac{\delta T}{T}$$

At 100 km, typical values are $T \cong 200$ K, $\bar{M} \cong 29$ g/mol, $g = 9.5$ m/s^2, so that $H \cong 6$ km. If $\delta T = 1$ K and $z - z_0 = 10$ km, then $\delta(\ln \rho) \cong \delta\rho/\rho \cong 0.83$ %. In the absence of compensating temperature perturbations at other altitudes, such a density perturbation will persist up into higher altitudes throughout the thermosphere.

MSIS 2.0 reproduces the temperatures much more accurately than NRLMSISE-00, with mean and StD of the difference equal 0.9 and 2.9 K versus 0.8 and 5.6 K for NRLMSISE-00. As discussed by Emmert et al. (2020, section 6.4) the improvement of temperature accuracy throughout the lower and middle atmosphere in MSIS 2.0 implies more accurate density at higher altitudes.

4. Summary and conclusions

Since 2000, density observations have been inferred from CHAMP, GRACE, and GOCE accelerometer data and Swarm GPS data, but these precise data of opportunity (except for Swarm, density derivation was not a mission objective) actually provide rather sparse coverage of the thermosphere over a solar cycle (c.f. Fig. 1). The overlaps in time and space of these most accurate datasets are rare, thus complicating their calibrations, which are necessary when fitting data to a thermosphere model for example, or when analyzing absolute instead of relative variations. The effect of the too few possible satellite comparisons on calibration is seen in the CNES GRACE data, which presents roughly-two levels when comparing to TLE2021 and HASDM. GRACE currently was only processed by CNES for the full mission, but without sophisticated aerodynamic models employed e.g. by TU Delft for CHAMP, GOCE and Swarm. Only the HASDM database provides almost full coverage of the 3D thermosphere for almost 2 solar cycles, but the provided uncertainty values for obvious reasons cannot be independently confirmed and the uncertainty description is lacking detail. Taking the spatial extent of HASDM into account, uncertainties and resolution are necessarily highly variable. We hope and recommend that a detailed description will be provided in the future so that this most complete density database available to the community can be fully exploited.

Large discrepancies among all datasets, on occasion in the tens of percent, are detected at all altitudes. The TLE2021 density is 2–12 % smaller on average than TLE2015, the largest offset being at 250 km. The difference between HASDM and TLE2021 density decreases with increasing altitude, from ~15 % at 250 km, ~6% at 400 km, to 0 % at 575 km. The altitude dependence of the offset is strongest at solar minimum. Comparisons of the satellite densities to TLE2021 and HASDM also revealed rather large differences, up to 15 % and 21 % on average, respectively. CHAMP and Swarm compared with

HASDM showed significant trends as well. Therefore, TLE2021 or HASDM should not be used for dataset calibration unless the aim is to adopt the scales of those datasets. TLE2021 at 475 and 575 km are equal to or a few percent smaller than HASDM, and Swarm A and B are 7 % and 3 % smaller on average than HASDM, so the agreement of the three datasets seems rather good at somewhat higher altitudes. However, the Swarm and HASDM density differences present an approximately linear drift in time. At 800 km, the difference between the Stella derived densities and HASDM is variable, with multi-annual and semi-annual periods revealed in the ratios displayed in Fig. 6. Compared to HASDM, the Stella densities range from 45 % smaller (2000–2003), to 8 % larger (2012–2016). The reasons for these differences are not well understood, but most likely are due to a combination of errors in solar radiation pressure modeling and aerodynamic drag modeling.

The comparisons presented in this study demonstrate that current density data cannot be simply assimilated, or combined, without first accurately calibrating them. However, accurate calibration is not always possible due to insufficient or no overlap between datasets, in which case only relative variations should be analyzed or fitted. Going forward, ensuring full data compatibility, requires that all density data providers employ physically accurate and harmonized aerodynamic force models. If not, new data cannot be exploited to the fullest. Secondly, the accuracy of the total density derivation procedures decreases with altitude, independent of the precision of the instrument to derive it (e.g. GNSS receiver or accelerometer), due to a diminishing drag signal even as radiation pressure remains almost constant, which makes longer averaging intervals necessary. More accurate modeling of the radiation pressure requires detailed information on the optical and thermal properties of the satellite surface, which is presently rarely available. Thirdly, the uncertainty should be described in detail, e.g. due to instrument, force model, and satellite model, and ideally be published with the density data.

At twenty years and counting, the TIMED-SABER data represent the longest-running, continuous dataset of temperature, pressure, and density in Earth's mesosphere and lower thermosphere (MLT). It is currently the only global source of mesosphere-lower thermosphere temperatures, which are of major importance for thermosphere modeling and assessment because of their significant impact on densities at higher altitude. Unfortunately, no follow-on mission is planned, and TIMED is well past its planned operational lifetime.

Declaration of Competing Interest

The authors declare that they have no known competing financial interests or personal relationships that could have appeared to influence the work reported in this paper.

Acknowledgements

References

Bettadpur, S., 2012 Gravity Recovery and Climate Experiment: Product Specification Document. Tech. Rep. GRACE 327-720 (CSR-GR-03-02), Rev. 4.6, Center for Space Research, The University of Texas at Austin, https://podaac-tools.jpl.nasa.gov/drive/files/allData/grace/-docs/ProdSpecDoc_v4.6.pdf.

Bowman, B.R., Tobiska, W.K., Marcos, F., Huang, C.Y., Lin, C.S., Burke, W.J., 2008. A New Empirical Thermospheric Density Model JB2008 Using New Solar and Geomagnetic Indices. In: Presentation at AIAA/AAS Astrodynamics Specialist Conference, Honolulu, Hawaii. https://doi.org/10.2514/6.2008-6438.

Bruinsma, S.L., 2015. The DTM-2013 thermosphere model. J. Space Weather Space Clim. 2, A04. https://doi.org/10.1051/swsc/2012005.

Bruinsma, S., Boniface, C., 2021. The DTM2020 thermosphere models. J. Space Weather Space Clim. 11, 47. https://doi.org/10.1051/swsc/2021032.

Bruinsma, S.L., Doornbos, E., Bowman, B.R., 2014. Validation of GOCE densities and thermosphere model evaluation. Adv. Space Res. 54, 576–585. https://doi.org/10.1016/j.asr.2014.04.008.

Bruinsma, S., Tamagnan, D., Biancale, R., 2004. Atmospheric densities derived from CHAMP/STAR accelerometer observations. Planet. Space Sci. 52, 297–312. https://doi.org/10.1016/j.pss.2003.11.004.

Bruinsma, S., Sutton, E., Solomon, S.C., Fuller-Rowell, T., Fedrizzi, M., 2018. Space Weather Modeling Capabilities Assessment: Neutral Density and Orbit Determination at LEO. Space Weather 16 (11), 1806–1816. https://doi.org/10.1029/2018SW002027.

Codrescu, S.M., Codrescu, M.V., Fedrizzi, M., 2018. An ensemble Kalman filter for the thermosphere-ionosphere. Space Weather 16 (1), 57–68. https://doi.org/10.1002/2017SW001752.

Crisp, N.H., Roberts, P.C.E., Livadiotti, S., et al., 2021. In-orbit aerodynamic coefficient measurements using SOAR (Satellite for Orbital Aerodynamics Research). Acta Astronaut. 180, 85–99. https://doi.org/10.1016/j.actaastro.2020.12.024.

Dawkins, E.C.M., Feofilov, A., Rezac, L., Kutepov, A.A., Janches, D., Höffner, J., et al., 2018. Validation of SABER v2.0 operational temperature data with ground-based lidars in the mesosphere-lower thermosphere region (75–105 km). J. Geophys. Res. 123, 9916–9934. https://doi.org/10.1029/2018JD028742.

Doornbos, E., 2011. Thermospheric density and wind determination from satellite dynamics, Ph.D. Dissertation, University of Delft, 188 pp. http://repository.tudelft.nl/.

Doornbos, E., Bruinsma, S., Fritsche, B., Koppenwallner, G., Visser, P., Van Den IJssel, J., de Teixeira de Encarnação, J, 2014. ESA contract 4000102847/NL/EL, GOCE+ Theme 3: Air density and wind retrieval using GOCE data – Final Report, TU Delft, https://earth.esa.int/eogateway/documents/20142/1181177/GOCE-theme-3-final-report.pdf.

Drinkwater, M.R., Floberghagen, R., Haagmans, R., Muzi, D., Popescu, A., 2003. GOCE: ESA's First Earth Explorer Core Mission. Space Sci. Rev. 108, 419–432. https://doi.org/10.1023/A:1026104216284.

Drob, D.P., Emmert, J.T., Meriwether, J.W., et al., 2015. An update to the Horizontal Wind Model (HWM): The quiet time thermosphere. Earth Space Sci. 2, 301–319. https://doi.org/10.1002/2014EA000089.

Emmert, J.T., 2009. A long-term data set of globally averaged thermospheric total mass density. J. Geophys. Res. 114, A06315. https://doi.org/10.1029/2009JA014102.

Emmert, J.T., 2015. Altitude and solar activity dependence of 1967–2005 thermospheric density trends derived from orbital drag. J. Geophys. Res. Space Physics 120, 2940–2950. https://doi.org/10.1002/2015JA021047.

Emmert, J.T., Drob, D.P., Picone, J.M., et al., 2020. NRLMSIS 2.0: A whole-atmosphere empirical model of temperature and neutral species densities e2020EA001321. Earth Space Sci. 8, 3. https://doi.org/10.1029/2020EA001321.

Emmert, J.T., Dhadly, M.S., Segerman, A.M., 2021. A globally averaged thermospheric density data set derived from two-line orbital element sets and special perturbations state vectors e2021JA029455. J. Geophys. Res. 126. https://doi.org/10.1029/2021JA029455.

Friis-Christensen, E., Lühr, H., Knudsen, D., Haagmans, R., 2008. Swarm – An Earth Observation Mission investigating Geospace. Adv. Space Res. 41 (1), 210–216. https://doi.org/10.1016/j.asr.2006.10.008.

Garcia-Comas, M., López-Puertas, M., Marshall, B.T., et al., 2008. Error in SABER temperature caused by non-LTE model parameters. J. Geophys. Res. 113, D24106. https://doi.org/10.1029/2008JD010105.

Jacchia, L.G., Slowey, J., 1963. Accurate drag determinations for eight artificial satellites : atmospheric densities and temperatures. Smithsonian Contrib. Astrophys. 8 (1), 1–99. https://doi.org/10.5479/si.00810231.8-1.1.

Klinger, B., Mayer-Gürr, T., 2016. The role of accelerometer data calibration within GRACE gravity field recovery: Results from ITSG-Grace2016. Adv. Space Res. 58 (9), 1597–1609. https://doi.org/10.1016/j.asr.2016.08.007.

Licata, R.J., Mehta, P.M., Tobiska, W.K., Bowman, B.R., Pilinski, M.D., 2021. Qualitative and quantitative assessment of the SET HASDM database. Space Weather 19. https://doi.org/10.1029/2021SW002798.

Livadiotti, S., Crisp, N.H., Roberts, P.C.E., et al., 2020. A review of gas-surface interaction models for orbital aerodynamics applications. Prog. Aerosp. Sci. 119. https://doi.org/10.1016/j.paerosci.2020.100675 100675.

Lühr, H., Grunwaldt, L., Förste, C, 2002. CHAMP Reference Systems, Transformations, and Standards. Tech. Rep. CH-GFZ-RS-002, Issue 2.3, http://op.gfz-potsdam.de/champ/docs_CHAMP/CH-GFZ-RS-002.PDF.

March, G., Doornbos, E., Visser, P., 2019. High-fidelity geometry models for improving the consistency of CHAMP, GRACE, GOCE and Swarm thermospheric density data sets. Adv. Space Res. 63 (1), 213–238. https://doi.org/10.1016/j.asr.2018.07.009.

Marsh, D.R., Mills, M.J., Kinnison, D.E., Lamarque, J.-F., 2013. Climate change from 1850 to 2005 simulated in CESM1 (WACCM). J. Clim. 26 (19), 7372–7391. https://doi.org/10.1175/JCLI-D-12-00558.1.

Mehta, P.M., Walker, A., McLaughlin, C.A., Koller, J., 2014. Comparing Physical Drag Coefficients Computed Using Different Gas-Surface Interaction Models. J. Spacecraft Rockets 51, 3. https://doi.org/10.2514/1.A32566.

Mehta, P.M., Paul, S.N., Crisp, N.H., Sheridan, P.L., Siemes, C., March, G., Bruinsma, S., 2023. Satellite drag coefficient modeling for thermosphere science and mission operations. Adv. Space Res. https://doi.org/10.1016/j.asr.2022.05.064.

Mertens, C.J., Mlynczak, M.G., López-Puertas, M., et al., 2001. Retrieval of mesospheric and lower thermospheric kinetic temperature from measurements of $CO2$ 15 μm Earth Limb Emission under non-LTE conditions. Geophys. Res. Lett. 28 (7), 1391–1394. https://doi.org/10.1029/2000GL012189.

Mostaza Prieto, D., Benjamin, G., Roberts, P., 2014. Spacecraft drag modeling. Prog. Aerosp. Sci. 64, 56–65. https://doi.org/10.1016/j.paerosci.2013.09.001.

Pearlman, M.R., Degnan, J.J., Bosworth, J.M., 2002. The International Laser Ranging Service. Adv. Space Res. 30 (2), 135–143. https://doi.org/10.1016/S0273-1177(02)00277-6.

Picone, J.M., Hedin, A.E., Drob, D.P., Aikin, A.C., 2002. NRLMSISE-00 empirical model of the atmosphere: Statistical comparisons and scientific issues. J. Geophys. Res. 107 (A12), 1468. https://doi.org/10.1029/2002JA009430.

Picone, J.M., Emmert, J.T., Lean, J.L., 2005. Thermospheric densities derived from spacecraft orbits: Accurate processing of two-line element sets. J. Geophys. Res. 110, A03301. https://doi.org/10.1029/2004JA010585.

Pilinski, M.D., Argrow, B.M., Palo, S.E., 2011. Drag coefficients of satellites with concave geometries: Comparing models and observations. J. Spacecraft and Rockets 48 (2), 312–325. https://doi.org/10.2514/1.50915.

Reigber, C., Bock, R., Förste, C., et al., 1996. CHAMP Phase B: Executive Summary, Scientific Technical Report STR; 96/13, Potsdam: GFZ German Research Centre for Geosciences, https://doi.org/10.2312/gfz.b103-96131.

Remsberg, E., Lingenfelser, G., Harvey, V.L., et al., 2003. On the verification of the quality of SABER temperature, geopotential height, and wind fields by comparison with Met Office assimilated analyses. J. Geophys. Res. 108 (D20), 4628. https://doi.org/10.1029/2003JD003720.

Remsberg, E.E., Marshall, B.T., García-Comas, M., et al., 2008. Assessment of quality of the Version 1.07 temperature versus pressure profiles of the middle atmosphere from TIMED/SABER. Geophys. Res. Lett. 113, D17101. https://doi.org/10.1029/2008JD010013.

Rezac, L., Kutepov, A., Russell III, J.M., Feofilov, A.G., Yue, J., Goldberg, R., 2015. Simultaneous retrieval of T(p) and $CO2$ VMR from two-channel non-LTE limb radiances and application to daytime SABER/TIMED. J. Atmos. and Sol. Terr. Phys., 130–131 https://doi.org/10.1016/j.jastp.2015.05.004.

Russell III, J.M., Mlynczak, M.G., Gordley, L.L., Tansock Jr., J.J., Esplin, R.W., 1999. Overview of the SABER experiment and preliminary calibration results. Proc. SPIE 3756, 277–288. https://doi.org/10.1117/12.366382.

Sentman, L.H., 1961. Comparison of the exact and approximate methods for predicting free molecule aerodynamic coefficients. ARS J. 31, 1576–1579.

Siemes, C., Encarnação, J., Doornbos, E., et al., 2016. Swarm accelerometer data processing from raw accelerations to thermospheric neutral densities, *Earth*. Planets and Space 68, 9. https://doi.org/10.1186/s40623-016-0474-5.

Siemes, C., 2019. Swarm satellite thermo-optical properties and external geometry, Tech. Rep. ESA-EOPG-MOM-MO-15, Issue 2.0, European Space Agency, https://earth.esa.int/eogateway/documents/20142/37627/swarm-thermo-optical-properties-and-external-geometry.pdf?-text=SWarm.

Storz, M.F., Bowman, B.R., Branson, M.J.I., Casali, S.J., Tobiska, W.K., 2005. High accuracy satellite drag model (HASDM). Adv. Space Res. 36 (12), 2497–2505. https://doi.org/10.1016/j.asr.2004.02.020.

Sutton, E.K., 2018. A new method of physics-based data assimilation for the quiet and disturbed thermosphere. Space Weather 16 (6), 736–753. https://doi.org/10.1002/2017SW001785.

Sutton, E.K., Forbes, J.M., Nerem, R.S., 2005. Global thermospheric neutral density and wind response to the severe 2003 geomagnetic storms from CHAMP accelerometer data. J. Geophys. Res. 110, A09S40. https://doi.org/10.1029/2004JA010985.

Tapley, B.D., Bettadpur, S., Watkins, M., Reigber, C., 2004. The gravity recovery and climate experiment: Mission overview and early results. Geophys. Res. Lett. 31, L09607. https://doi.org/10.1029/2004GL019920.

Tobiska, W.K., Bowman, B.R., Bouwer, S.D., et al., 2021. The SET HASDM density database. Space Weather 19, 4. https://doi.org/10.1029/2020SW002682.

Van den Ijssel, J., Doornbos, E., Iorfida, E., March, G., Siemes, C., Montenbrück, O., 2020. Thermosphere densities derived from Swarm GPS observations. Adv. Space Res. 65 (7), 1758–1771. https://doi.org/10.1016/j.asr.2020.01.004.

Van Helleputte, T., Doornbos, E., Visser, P., 2009. CHAMP and GRACE accelerometer calibration by GPS-based orbit determination. Adv. Space Res. 43 (12), 1890–1896. https://doi.org/10.1016/j.asr.2009.02.017.

Vielberg, K., Kusche, J., 2020. Extended forward and inverse modeling of radiation pressure accelerations for LEO satellites. J. Geod. 94, 43. https://doi.org/10.1007/s00190-020-01368-6.

Visser, P.N.A., Van Den Ijssel, J., 2016. Calibration and validation of individual GOCE accelerometers by precise orbit determination. J. Geod. 90, 1–13. https://doi.org/10.1007/s00190-015-0850-0.

Wöske, F., Kato, T., Rievers, B., List, M., 2019. GRACE accelerometer calibration by high precision non-gravitational force modeling. Adv. Space Res. 63 (3), 1318–1335. https://doi.org/10.1016/j.asr.2018.10.025.